Conductivity tensor of anisotropic composite media from the microstructure

S. Torquato
Department of Mechanical and Aerospace Engineering and Department of Chemical Engineering, North Carolina State University, Raleigh, North Carolina 27695-7910

Asok K. Sen[a)]
Department of Mechanical and Aerospace Engineering, North Carolina State University, Raleigh, North Carolina 27695-7910

(Received 27 July 1989; accepted for publication 2 October 1989)

Perturbation expansions and rigorous bounds on the effective conductivity tensor σ_e of d-dimensional anisotropic two-phase composite media of arbitrary topology have recently been shown by the authors to depend upon the set of n-point probability functions $S_1^{(i)},...,S_n^{(i)}$. $S_n^{(i)}$ gives the probability of simultaneously finding n points in phase i ($i = 1,2$). Here we describe a means of representing these statistical quantities for distributions of identical, oriented inclusions of arbitrary shape. Our results are applied by computing second-order perturbation expansions and bounds for a certain distribution of oriented cylinders with a finite aspect ratio. We examine both cases of conducting cylindrical inclusions in an insulating matrix and of insulating *cracks* or *voids* in a conducting matrix.

I. INTRODUCTION

The problem of relating the macroscopic properties of a heterogeneous (or composite) material to its microstructure is a long-standing one in science, attracting the attention of Maxwell,[1] Rayleigh,[2] and Einstein.[3] In this paper, we focus on studying the microstructure and the effective electrical (or thermal) conductivity tensor σ_e of a random d-dimensional two-phase anisotropic composite medium. Examples of anisotropic composite materials include distributions of oriented, nonspherical inclusions (e.g., short-fiber composites), layered media (e.g., sandstones and laminates), etc. For macroscopically isotropic two-phase composites (i.e., $\sigma_e = \sigma_e$ U, where U is the unit dyadic), considerable advances in predicting σ_e have been made[4–6] since the pioneering paper of Brown[7] in which it was shown that σ_e depends upon an infinite set of correlation functions that statistically characterize the composite.

The rigorous determination of the conductivity tensor σ_e for the more complicated case of a macroscopically anisotropic composite has been less comprehensively studied. Rocha and Acrivos[8] determined σ_e for infinitely dilute dispersions containing inclusions of arbitrary shape. Hori[9] developed perturbation expansions and bounds for σ_e which, as indicated below, have some undesirable features. Willis[10] derived bounds on σ_e for composites containing aligned, ellipsoidal inclusions which depend upon the microgeometry via the shape of the inclusions and volume fraction only. More recent work includes the development of Hashin–Shtrikman-type bounds by Kohn and Milton[11] and the powerful continued-fractions approach to bounds of Milton[4]; see also references contained therein.

Sen and Torquato[12] very recently derived a new perturbation expansion for the conductivity tensor σ_e of a macroscopically anisotropic d-dimensional two-phase composite of arbitrary topology. The nth-order tensor coefficients $A_n^{(i)}$ of the expansion are absolutely convergent multidimensional integrals over the set of n-point probability functions $S_1^{(i)},...,S_n^{(i)}$ of the medium in contrast to the work of Hori.[13] The quantity $S_n^{(i)}(\mathbf{x}_1,...,\mathbf{x}_n)$ gives the probability of finding n points at positions $\mathbf{x}_1,...,\mathbf{x}_n$, respectively, simultaneously in phase i ($i = 1,2$). The tensors $A_n^{(i)}$ are shown[12] to be related to Milton's[4] weights and normalization factors, and thus the latter quantities (for $n = 2$, 3, and 4) have been given explicitly in terms of integrals over the $S_n^{(i)}$ for the first time. Sen and Torquato[12] then derived new, rigorous nth-order bounds on σ_e that depend upon the n-point parameters $A_n^{(i)}$ for $n = 2$, 3, and 4. Thus, in order to compute perturbation expansions or bounds, one must have knowledge of the $S_n^{(i)}$ which, until recently, were difficult to ascertain.

The present paper has a twofold objective. First, we describe a means of representing and computing the n-point probability functions for anisotropic media comprised of a distribution of oriented, arbitrary-shaped inclusions of one type of material (or void) in a matrix of another material. Laying this groundwork then enables one to compute the perturbation-expansion tensor coefficients and bounds for σ_e. Second, we apply the aforementioned results by evaluating the two-point parameter $A_2^{(i)}$ for a certain distribution of oriented cylinders of a finite aspect ratio. Such an evaluation enables us to compute second-order perturbation expansions and bounds for this model. We consider both cases of conducting inclusions in an insulating matrix and of insulating inclusions (i.e., cracks or voids) in a conducting matrix.

Finally, we note that, for reasons of mathematical analogy, the general results for the conductivity tensor given here translate immediately into equivalent results for the dielectric constant, diffusion coefficient, and magnetic permeability tensors of such composites.

[a)] Present address: Dept. of Chemical Engineering, University of Houston, Houston, TX 77204-4792.

 0021-8979/90/031145-11$03.00

II. CONDUCTIVITY TENSOR: PERTURBATION EXPANSIONS AND BOUNDS

Sen and Torquato[12] have derived perturbation expansions and rigorous bounds for the effective conductivity tensor $\boldsymbol{\sigma}_e$ of two-phase anisotropic composite media of arbitrary topology and dimensionality d. The composite medium is a domain of space D of d-dimensional volume V which is subdivided into two phases: one phase D_1, characterized by volume fraction ϕ_1 and isotropic conductivity σ_1, and another phase D_2, characterized by a volume fraction ϕ_2 and isotropic conductivity σ_2. The local conductivity at position $\mathbf{x}$ is given by the scalar function

$$\sigma(\mathbf{x}) = \sigma_j + (\sigma_i - \sigma_j) I^{(i)}(\mathbf{x}), \quad i \neq j, \tag{1}$$

where the characteristic function of phase i is

$$I^{(i)}(\mathbf{x}) = \begin{cases} 1, & \mathbf{x} \in D_i \\ 0, & \text{otherwise.} \end{cases} \tag{2}$$

As indicated above, each phase is isotropic and hence macroscopic anisotropy arises out of some asymmetry in the microstructure, i.e., due to statistical anisotropy, such as a distribution of oriented nonspherical inclusions in a matrix, layered media, such as sandstones and laminates, etc. For the purposes of the present work, it is useful to summarize some of the findings of Ref. 12.

A. Perturbation expansions

Sen and Torquato[12] found the following perturbation expansion involving the conductivity tensor:

$$(\beta_{ij}\phi_i)^2(\boldsymbol{\sigma}_e - \sigma_j \mathsf{U})^{-1}[\boldsymbol{\sigma}_e + (d-1)\sigma_j \mathsf{U}] = \phi_i \beta_{ij} \mathsf{U} - \sum_{n=2}^{\infty} \mathsf{A}_n^{(i)} \beta_{ij}^n, \quad i \neq j, \tag{3}$$

where

$$\beta_{ij} = \frac{\sigma_i - \sigma_j}{\sigma_i + (d-1)\sigma_j},$$

and the tensor coefficients $\mathsf{A}_n^{(i)}$ are volume integrals over the set of n-point probability functions $S_1^{(i)},\ldots,S_n^{(i)}$ associated with the phase i. Relation (3) actually represents two series expansions, one for $i=1$ and $j=2$, and the other for $i=2$ and $j=1$. The n-point probability function

$$S_n^{(i)}(\mathbf{x}^n) \equiv \left\langle \prod_{j=1}^{n} I^{(i)}(\mathbf{x}_j) \right\rangle \tag{4}$$

gives the probability of finding n points with positions $\mathbf{x}^n \equiv \{\mathbf{x}_1,\ldots,\mathbf{x}_n\}$ all in phase i. For statistically anisotropic but homogeneous media, the $S_n^{(i)}$ depend upon the relative displacements $\mathbf{x}_{ij} = \mathbf{x}_j - \mathbf{x}_i$, so that, for example, $S_1^{(i)}$ equals the volume fraction of phase i, ϕ_i. The angular brackets in relation (4) denote an ensemble average. The general expression for the symmetric tensor coefficients $\mathsf{A}_n^{(i)}$ (also referred to as n-point microstructural parameters) are given explicitly in Ref. 12. The n-point tensors $\mathsf{A}_n^{(i)}$ $(n=2,3,\ldots)$ generally will not possess common principal axes. This implies that for general media the principal axes of the macroscopic conductivity tensor $\boldsymbol{\sigma}_e$ will rotate as the phase conductivity ratio changes, such as composites with chirality, i.e., composites with some degree of left- or right-handed asymmetry.[14] There exists a large class of media, however, which, in fact, do possess the symmetry required for all the $\mathsf{A}_n^{(i)}$ to possess common principal axes (e.g., a random array of oriented, identical ellipsoids in a matrix). It is useful here to write out the first few n-point microstructural parameters for statistically anisotropic but homogeneous media[12]:

$$\mathsf{A}_2^{(i)} = \frac{d}{2\pi(d-1)} \int_{\delta} d\mathbf{x}\ \mathsf{t}(\mathbf{x}) [S_2^{(i)}(\mathbf{x}) - \phi_i^2], \tag{5}$$

$$\mathsf{A}_3^{(i)} = \left(\frac{d}{2\pi(d-1)}\right)^2 \int d\mathbf{x}_2\, d\mathbf{x}_3\, \mathsf{t}(\mathbf{x}_{12}) \cdot \mathsf{t}(\mathbf{x}_{23}) \left(S_3^{(i)}(\mathbf{x}_{12},\mathbf{x}_{13}) - \frac{S_2^{(i)}(\mathbf{x}_{12}) S_2^{(i)}(\mathbf{x}_{23})}{\phi_i} \right), \tag{6}$$

$$\mathsf{A}_4^{(i)} = \left(\frac{d}{2\pi(d-1)}\right)^3 \int d\mathbf{x}_2\, d\mathbf{x}_3\, d\mathbf{x}_4\, \mathsf{t}(\mathbf{x}_{12}) \cdot \mathsf{t}(\mathbf{x}_{23}) \cdot \mathsf{t}(\mathbf{x}_{34}) \left(S_4^{(i)}(\mathbf{x}_{12},\mathbf{x}_{13},\mathbf{x}_{14}) - \frac{S_3^{(i)}(\mathbf{x}_{12},\mathbf{x}_{13}) S_2^{(i)}(\mathbf{x}_{34})}{\phi_i} - \frac{S_3^{(i)}(\mathbf{x}_{23},\mathbf{x}_{24}) S_2^{(i)}(\mathbf{x}_{12})}{\phi_i} + \frac{S_2^{(i)}(\mathbf{x}_{12}) S_2^{(i)}(\mathbf{x}_{23}) S_2^{(i)}(x_{34})}{\phi_i^2} \right) \tag{7}$$

where

$$\mathsf{t}(\mathbf{x}) = \frac{d\mathbf{x}\mathbf{x} - x^2 \mathsf{U}}{x^{d+2}}, \tag{8}$$

and U is the unit dyadic. The subscript δ on the integral of (5) (which is to be integrated over the sample volume V) indicates that it is to be carried out with the exclusion of an infinitesimally small d-dimensional sphere centered at $\mathbf{x}$.[12]

Tensor properties of the $\mathsf{A}_n^{(i)}$ were studied in Ref. 12. We shall not repeat these here but shall briefly describe some important ones for the two-point parameter $\mathsf{A}_2^{(i)}$ in particular since we will use them in Sec. IV. First we note that $\mathsf{A}_2^{(i)} = 0$ for macroscopically isotropic media. Second, unlike the other parameters, $\mathsf{A}_2^{(1)} = \mathsf{A}_2^{(2)}$, and thus we shall henceforth denote $\mathsf{A}_2^{(i)}$ by A_2. Third, A_2 is traceless. Fourth, the following bounds on A_2 (and related parameters) are satisfied:

$$-(d-1)\phi_1\phi_2 \leqslant (A_2)_{kk} \leqslant \phi_1\phi_2, \tag{9a}$$

$$0 \leqslant (A_2^*)_{kk} \leqslant 1, \tag{9b}$$

$$-\phi_1\phi_2 \leqslant (a_2^{(i)})_{kk} \leqslant 0, \tag{9c}$$

where $(B)_{kk}$ $(k=1,\ldots,d)$ denotes the diagonal elements of the diagonalized form of a tensor B, A_2^* is the *depolarization tensor*[12] (with unit trace) simply related to A_2 by

$$\mathsf{A}_2^* = \frac{1}{d}\left(\mathsf{U} - \frac{1}{\phi_1\phi_2}\mathsf{A}_2\right), \tag{10}$$

and $\mathsf{a}_2^{(i)}$ is the tensor (with trace equal to $-\phi_1\phi_2$) defined by Eq. (12) below.

Sen and Torquato[12] used relation (3) to obtain an expansion of the effective conductivity tensor in powers of $\delta_{ij} = (\sigma_i - \sigma_j)/\sigma_j$. (Note that δ_{ij} is not the Kronecker delta.) Employing Eq. (3) we found through fourth order that

$$\sigma_e/\sigma_j = \mathsf{U} + \mathsf{a}_1^{(i)}\delta_{ij} + \mathsf{a}_2^{(i)}\delta_{ij}^2 + \mathsf{a}_3^{(i)}\delta_{ij}^3 + \mathsf{a}_4^{(i)}\delta_{ij}^4 + O(\delta_{ij}^5), \quad i \neq j, \tag{11}$$

where

$$\mathsf{a}_1^{(i)} = \phi_i\mathsf{U}, \tag{12}$$

$$\mathsf{a}_2^{(i)} = -\phi_1\phi_2\mathsf{A}_2^*, \tag{13}$$

$$\mathsf{a}_3^{(i)} = (1/d^2)(d\phi_i\phi_j^2\mathsf{A}_2^* + \mathsf{A}_3^{(i)}), \tag{14}$$

and

$$\mathsf{a}_4^{(i)} = (1/d^3)[-d^3\phi_i\phi_j^3(\mathsf{A}_2^*)^3 - d\phi_j\mathsf{A}_2^*\cdot\mathsf{A}_3^{(i)} - d\phi_j\mathsf{A}_3^{(i)}\cdot\mathsf{A}_2^* - \mathsf{A}_3^{(i)} + \mathsf{A}_4^{(i)}]. \tag{15}$$

The n-point microstructural parameters $\mathsf{a}_n^{(i)}$ will be of use in expressing rigorous bounds on σ_e.

B. Rigorous bounds

Until recently, knowledge of lower-order n-point probability functions (i.e., $S_1^{(i)}$, $S_2^{(i)}$, $S_3^{(i)}$, and $S_4^{(i)}$) even for macroscopically *isotropic* media has been viturally nonexistent, either theoretically or experimentally.[15] In the last several years, considerable advances have been made along these lines both theoretically[16,17] and experimentally,[18] and as a result, effective isotropic property relations which depend upon such information have been computed.[18,19] It appears, however, that the determination of the $S_n^{(i)}$ for $n \geqslant 5$ of arbitrary media is beyond presently available technology. Thus, series representations of σ_e such as (3) and (11) cannot be exactly summed. Rigorous methods to estimate σ_e must necessarily involve limited microstructural information.

If we accept our inability to obtain exact solutions for σ_e for arbitrary topologies, then any rigorous statement about σ_e must be in the form of an inequality, i.e., a rigorous bound. Bounds on effective properties are useful since: (i) they may be used to test the merits of a theory or computer experiment; (ii) as successfully more microstructural information is included, the bounds become progressively narrower; and (iii) one of the bounds can typically provide a good estimate of the effective property, for a wide range of volume fractions, even when the reciprocal bound diverges from it.[5]

Sen and Torquato[12] have derived nth-order bounds on σ_e that depend upon the n-point microstructural parameters $\mathsf{A}_n^{(i)}$, or equivalent $\mathsf{a}_n^{(i)}$, for $n = 1, 2, 3$, and 4. The results for $n = 2$, 3, and 4 are new. *nth-order* bounds are exact through order $\delta_{ij}(\sigma_i - \sigma_j)/\sigma_j$.

1. First-order bounds

The first-order lower and upper bounds are, respectively, given by

$$\sigma_e^{(1L)} = \frac{\sigma_1\sigma_2}{\sigma_1\phi_2 + \sigma_2\phi_1}\mathsf{U}, \tag{16}$$

$$\sigma_e^{(1U)} = (\sigma_1\phi_1 + \sigma_2\phi_2)\mathsf{U}. \tag{17}$$

Equations (16) and (17), which represent the harmonic and arithmetic means of the local conductivity, respectively, were first derived by Wiener[20] in the isotropic context. They are exactly attained for parallel slab geometries: (16) being the case in which the applied field is directed perpendicular to the slabs—the law of "series resistances"—and (17) being the case in which the applied field is directed along the slabs—the law of "parallel resistances."

2. Second-order bounds

Second-order bounds are found to be[12]

$$\frac{\sigma_e^{(2)}}{\sigma_j} = \left[\mathsf{U} + \left(\phi_i\mathsf{U} - \frac{1}{\phi_i}\mathsf{a}_2^{(i)}\right)\delta_{ij}\right] \times \left(\mathsf{U} - \frac{1}{\phi_i}\mathsf{a}_2^{(i)}\delta_{ij}\right)^{-1}. \tag{18}$$

Here $\mathsf{a}_2^{(i)}$ is given by Eq. (13). Equation (18) for $\sigma_2 \geqslant \sigma_1$ (as described below) gives a lower bound $\sigma_e^{(2L)}$ for $j = 1$ and $i = 2$ and an upper bound $\sigma_e^{(2U)}$ for $j = 2$ and $i = 1$. It should be noted that these bounds for macroscopically isotropic media reduce to the well-known Hashin–Shtrikman ($d = 3$) and Hashin ($d = 2$) isotropic bounds.[21] For a distribution of inclusions of arbitrary shape and size (phase 2), the bounds (18) are exact to first order in the inclusion volume fraction ϕ_2. Note that if the upper bound of $\mathsf{a}_2^{(i)}$ for one of its principal directions is achieved, i.e., if $(a_2^{(i)})_{kk} = 0$ or, equivalently, $(A_2)_{kk} = \phi_1\phi_2$ or $(A_2^*)_{kk} = 0$ [cf. Eq. (9)], then the second-order bounds on $(\sigma_e)_{kk}$ coincide and equal $\sigma_1\phi_1 + \sigma_2\phi_2$, which is exactly the first-order upper bound (17). This corresponds to the conductivity for parallel slabs or infinitely long, parallel needles (rods) in the parallel direction. Furthermore, if the reciprocal bounds of (9) are achieved [i.e., if $(a_2^{(i)})_{kk} = -\phi_1\phi_2$, $(A_2^*)_{kk} = 1$ or $(A_2)_{kk} = -(d-1)\phi_1\phi_2$], then the second-order bounds on $(\sigma_e)_{kk}$ coincide and equal $\sigma_1\sigma_2/(\sigma_1\phi_2 + \sigma_2\phi_1)$ which, not surprisingly, is exactly the first-order lower bound (16).

3. Third-order bounds

The third-order lower bound is given by[12]

$$(\sigma_e^{(3L)}/\sigma_2)^{-1} = (1 + \phi_1\delta_{21})\mathsf{U} + \delta_{21}^2\mathsf{c}_2\cdot[(1 - \phi_1\delta_{21})\mathsf{c}_2 + (\mathsf{b}_3 + \phi_1\mathsf{b}_2)\delta_{21}]^{-1}\cdot\mathsf{c}_2, \tag{19}$$

where

$$\mathsf{b}_2 = \phi_1\mathsf{U} + \mathsf{a}_2^{(1)}, \tag{20}$$

$$\mathsf{c}_2 = \phi_1^2\mathsf{U} - \mathsf{b}_2, \tag{21}$$

and

$$\mathsf{b}_3 = -(\phi_1\mathsf{U} + 2\mathsf{a}_2^{(1)} + \mathsf{a}_3^{(1)}). \tag{22}$$

The third-order upper bound is[12]

$$\sigma_e^{(3U)}/\sigma_1 = (1 + \phi_2\delta_{21})\mathsf{U} + \delta_{21}^2\mathsf{a}_2^{(2)}\cdot(\mathsf{a}_2^{(2)} - \mathsf{a}_3^{(2)}\delta_{21})^{-1}\cdot\mathsf{a}_2^{(2)}, \tag{23}$$

where $a_2^{(i)}$ and $a_3^{(i)}$ are given by Eqs. (13) and (14), respectively. We note that for isotropic media, these bounds reduce to the well-known Beran[22] and Silnutzer[23] bounds for $d = 3$ and 2, respectively.

4. Fourth-order bounds

The fourth-order bounds are given by[12]

$$\sigma_e/\sigma_j = \tfrac{1}{2}\mathsf{A}\mathsf{B}^{-1} + \tfrac{1}{2}(\mathsf{A}\mathsf{B}^{-1})^T, \tag{24}$$

where

$$\mathsf{A} = \mathsf{U} + \mathsf{p}_1^{(i)}\delta_{ij} + \mathsf{p}_2^{(i)}\delta_{ij}^2, \tag{25}$$

$$\mathsf{B} = (\mathsf{U} + \mathsf{q}_1^{(i)}\delta_{ij} + \mathsf{q}_2^{(i)}\delta_{ij}^2)^{-1}, \tag{26}$$

$$\mathsf{p}_1^{(i)} = \mathsf{a}_1^{(i)} + \mathsf{q}_1^{(i)}, \tag{27}$$

$$\mathsf{p}_2^{(i)} = \mathsf{a}_2^{(i)} - \phi_i^{-1}\mathsf{a}_3^{(i)} + [\mathsf{a}_1^{(i)} - \phi_i^{-1}\mathsf{a}_2^{(i)}]\cdot\mathsf{q}_1^{(i)}, \tag{28}$$

$$\mathsf{q}_1^{(i)} = [\mathsf{a}_2^{(i)}\cdot\mathsf{a}_2^{(i)} - \phi_i\mathsf{a}_3^{(i)}]^{-1} \cdot[\mathsf{a}_1^{(i)}\cdot\mathsf{a}_4^{(i)} - \mathsf{a}_2^{(i)}\cdot\mathsf{a}_3^{(i)}], \tag{29}$$

and

$$\mathsf{q}_2^{(i)} = -\phi_i^{-1}(\mathsf{a}_3^{(i)} + \mathsf{a}_2^{(i)}\cdot\mathsf{q}_1^{(i)}). \tag{30}$$

Equation (24) for $\sigma_2 \geqslant \sigma_1$ gives an upper bound $\sigma_e^{(4U)}$ for $i = 1, j = 2$ and $\sigma_e^{(4L)}$ for $i = 2, j = 1$. In the isotropic limit, these bounds reduce to the fourth-order bounds derived by Milton.[24] For anisotropic media in which the microstructural tensors possess *common principal axes* (i.e., when they commute), relation (24) has been shown to be a rigorous bound. Such symmetric media include random, oriented inclusions of arbitrary shape and size as a special case. In light of the above arguments, Sen and Torquato[12] conjectured that (24) represents rigorous fourth-order bounds for general (asymmetric) anisotropic media.

5. Utility of lower-order bounds

It is instructive to comment on the practical use of rigorous lower-order bounds (such as second-, third-, and fourth-order bounds) in predicting the conductivity tensor when one of the phases (say phase i) is much more conducting than the other phase (phase j), i.e., if $\sigma_i \gg \sigma_j$, $i \neq j$. In such situations, upper bounds on $(\sigma_e)_{kk}/\sigma_j$ (for $\phi_i > 0$) become very large and in the limit $\sigma_i/\sigma_j \to \infty$ become infinite in order to take into account the possibility of a realization in which the conducting phase is percolating in the x_i direction ($i = 1$, 2, or 3). In contrast, for most geometries, the lower bounds on $(\sigma_e)_{kk}/\sigma_j$ remain finite for $0 < \phi_i < 1$ even when $\sigma_i/\sigma_j \to \infty$. For geometries in which the lower bounds on $(\sigma_e)_{kk}/\sigma_j$ become infinite in the limit $\sigma_i/\sigma_j \to \infty$, the lower bounds are obviously *exact* since they coincide with the upper bounds. (Examples of geometries for which the bounds coincide have already been described in Sec. II B 2.) Note that if the bounds on $(\sigma_e)_{kk}$ are scaled by σ_i instead of σ_j in these instances, then (for most geometries) the upper bounds remain finite and the lower bounds become small, approaching *zero* in the limit $\sigma_i/\sigma_j \to \infty$.

Some investigators have dismissed bounds as impractical because of the divergence in the bounds when $\sigma_i \gg \sigma_j$. However, as noted at the beginning of this subsection, one of the bounds can typically provide a good estimate of the effective conductivity in such instances. For $\sigma_i \gg \sigma_j$ and $0 < \phi_i < 1$, the lower bound $(\sigma_e^{(L)})_{kk}$ will yield a reasonable estimate of $(\sigma_e)_{kk}$ provided that the conducting phase, in general, does not possess large *connected* substructures in the x_i direction. (As noted above, however, there are cases in which the bounds coincide for geometries in which the conducting phase is continuously connected.) If the conducting phase is continuously connected, then the upper bound $(\sigma_e^{(U)})_{kk}$ will provide a good estimate of $(\sigma_e)_{kk}$.

III. n-POINT PROBABILITY FUNCTIONS

A. Series representation for oriented inclusions

The effective conductivity tensor σ_e is seen to depend upon the infinite set of n-point probability functions, i.e., $S_1^{(i)},\ldots,S_n^{(i)}$ $(n \to \infty)$. Observe that the n-point probability function for phase 1, $S_n^{(1)}$, is simply related to the phase 2 counterpart, $S_n^{(2)}$.[16] Here we shall consider the determination of this set of functions for anisotropic media composed of identical, oriented inclusions of arbitrary shape (phase 2) distributed throughout some other material that we generically refer to as matrix (phase 1). (Note that the matrix need not be continuously connected.) Recall that for this large class of materials the n-point microstructural tensors, $\mathsf{A}_n^{(i)}$ or $\mathsf{a}_n^{(i)}$, commute.

Torquato and Stell[16] were actually the first to represent $S_n^{(i)}$ (for any n) for the nontrivial microgeometry of a statistically inhomogeneous distribution of N d-dimensional spheres in terms of the n-particle probability density functions $\rho_1,\ldots,\rho_n$. The quantity $\rho_n(\mathbf{r}^n)$ characterizes the probability of finding a configuration of n spheres with positions $\mathbf{r}^n \equiv \{\mathbf{r}_1,\ldots,\mathbf{r}_n\}$. Using these general results, lower-order $S_n^{(i)}$ for distributions of overlapping as well as nonoverlapping spheres and disks were computed.[17,19] It is important to note that their general results are actually not only applicable to spheres but (after an appropriate generalization of the *inclusion indicator function*) to any microgeometry composed of identical inclusions in which each configurational coordinate $\mathbf{r}_i$ is fully specified by its center-of-mass position. This class of materials includes oriented rectangles, ellipses, etc., in two dimensions and oriented rectangular parallelpipeds, ellipsoids, cylinders, etc., in three dimensions.

For this class of microstructures, the results of Torquato and Stell[16] together with the aforementioned observations lead to the explicit representation

$$S_n^{(1)}(\mathbf{x}^n) = 1 + \sum_{k=1}^{N} \frac{(-1)^k}{k!} \int \rho_k(\mathbf{r}^k) \times \prod_{j=1}^{k}\left(1 - \prod_{i=1}^{n}[1 - m(\mathbf{x}_i - \mathbf{r}_j)]\right) d\mathbf{r}_j \tag{31}$$

for the matrix phase, where

$$m(\mathbf{x}) = \begin{cases} 1, & \mathbf{x} \in D_I \\ 0, & \text{otherwise} \end{cases} \tag{32}$$

is the inclusion indicator function, D_I the inclusion region, and $\mathbf{x}$ a position vector measured with respect to the inclusion centroid. For a disk or sphere of radius a, the particle indicator function is particularly simple:

$$m(\mathbf{x}) = \begin{cases} 1, & x > a \\ 0, & x > a, \end{cases} \tag{33}$$

where $x \equiv |\mathbf{x}|$.

For nonspherical shapes, $m(\mathbf{x})$ is more complicated. For example, for a rectangle having sides of lengths $2a$ and $2b$ (as indicated in Fig. 1),

$$m(\mathbf{x}) = \begin{cases} 1, & |x_1| < a \text{ and } |x_2| < b \\ 0, & \text{otherwise.} \end{cases} \tag{34}$$

For an ellipse with axes of lengths $2a$ and $2b$, respectively (see Fig. 1),

$$m(\mathbf{x}) = \begin{cases} 1, & \dfrac{x_1^2}{a^2} + \dfrac{x_2^2}{b^2} < 1 \\ 0, & \text{otherwise.} \end{cases} \tag{35}$$

The inclusion indicator function for a rectangular parallelepiped having sides of length $2a$, $2b$, and $2c$ is given by

$$m(\mathbf{x}) = \begin{cases} 1, & |x_1| < a \text{ and } |x_2| < b \text{ and } |x_3| < c \\ 0 & \text{otherwise.} \end{cases} \tag{36}$$

For an ellipsoidal inclusion with axes of lengths a, b, and c (see Fig. 2),

$$m(\mathbf{x}) = \begin{cases} 1, & \dfrac{x_1^2}{a^2} + \dfrac{x_2^2}{b^2} + \dfrac{x_3^2}{c^2} < 1 \\ 0, & \text{otherwise.} \end{cases} \tag{37}$$

Finally, as a last example, the inclusion indicator function for a circular cylinder of diameter $2a$ and length $2b$ (see Fig. 2) is

$$m(\mathbf{x}) = \begin{cases} 1, & x_1^2 + x_2^2 < a^2 \text{ and } |x_3| < b \\ 0, & \text{otherwise.} \end{cases} \tag{38}$$

To summarize, Eq. (31) is valid for general inhomogeneous arrays of identical, oriented inclusions of arbitrary shape distributed throughout a matrix with an arbitrary degree of mutual penetrability. Information about interparticle interactions (mutual attraction and repulsion) enters though the n-particle probability density functions $\rho_1,\ldots,\rho_n$.

If the medium is statistically homogeneous but anisotropic, then the n-particle probability density and n-point probability function are translationally invariant and hence just depend upon the relative displacements, i.e., $\rho_n(\mathbf{r}_{12},\ldots,\mathbf{r}_{1n})$ and $S_n^{(i)} = S_n^{(i)}(\mathbf{x}_{12},\ldots,\mathbf{x}_{1n})$ where $\mathbf{r}_{1i} = \mathbf{r}_i - \mathbf{r}_1$ and $\mathbf{x}_{1i} = \mathbf{x}_i - \mathbf{x}_1$. Statistical homogeneity implies that the *thermodynamic limit* has been taken i.e., $N \to \infty$, $V \to \infty$ such that $\rho = N/V = \rho_1(\mathbf{r}_1)$ is some finite constant (ρ being the number density). For such media, $S_1^{(i)}$ is simply equal to the volume fraction ϕ_i of the ith phase.

For homogeneous distributions of oriented inclusions which are allowed to *overlap* or *fully penetrate* one another, the n-particle probability densities are especially simple, i.e., $\rho_n(r^n) = \rho^n$ since the positions of the inclusion centroids are spatially uncorrelated (they are Poisson distributed). As described below, for such models, the integrals of Eq. (31) are straightforward to evaluate. On the other hand, if the inclusions are mutually impenetrable (and possess interparticle attraction), the ρ_n are generally very complex, especially for $n \geqslant 3$.

Given the theoretical framework to represent the $S_n^{(i)}$ described above, one can now, in principle, compute the perturbation expansions and the bounds described in Sec. II for distributions of oriented, identical inclusions of arbitrary shape. We now derive and discuss some specific results for the $S_n^{(i)}$.

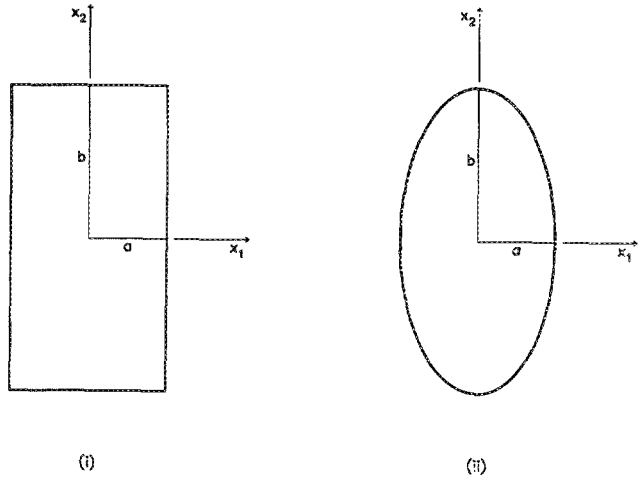

FIG. 1. Examples of two-dimensional inclusions: (i) Rectangle with slides of lengths 2a and 2b; (ii) ellipse with axes of lengths 2a and 2b.

B. Dilute distributions of oriented inclusions

For a dilute, homogeneous distribution of oriented inclusions which interact with an arbitrary interparticle potential, one can evaluate Eq. (31) for the matrix n-point probability function for any n. Through order ρ, we have exactly from Eq. (31) that

$$\begin{aligned} S_n^{(1)}(\mathbf{x}_{1n},\ldots,\mathbf{x}_{1n}) &= 1 - \rho \int \left(1 - \prod_{i=1}^{n} [1 - m(\mathbf{x}_i - \mathbf{r}_1)]\right) d\mathbf{r}_1, \\ &= 1 - \rho V_n(\mathbf{x}_{12},\ldots,\mathbf{x}_{in}). \end{aligned} \tag{39}$$

The integral of Eq. (39) is recognized to be the union volume of n regions (each of which have precisely the same shape, size, and orientation of an inclusion) whose centroids are separated by the displacements $\mathbf{x}_{12},\ldots,\mathbf{x}_{1n}$. We shall denote this union volume by $V_n(\mathbf{x}_{12},\ldots,\mathbf{x}_{1n})$. It must be emphasized that the origin of V_n has nothing whatsoever to do with the penetrability of inclusions but rather arises because of volume excluded to "point" particles by the inclusions. For $n = 1$, V_1 is simply the volume of an inclusion. In the case of $n = 2$, for example, the union volumes of two inclusion regions for rectangular and circular cylindrical inclusions (cf. Figs. 1 and 2) are given, respectively, by

$$\begin{aligned} V_2(\mathbf{x}) &= 4a^2b^2 - (2a - x)(2b - y) \\ &\quad \times H(2a - x)H(2b - y), \end{aligned} \tag{40}$$

$$\begin{aligned} V_2(\mathbf{x}) &= 4\pi a^2 b^2 - (2b - |x\cos\theta|)A(|x\sin\theta|) \\ &\quad \times H(2a - |x\sin\theta|)H(2b - |x\cos\theta|), \end{aligned} \tag{41}$$

where

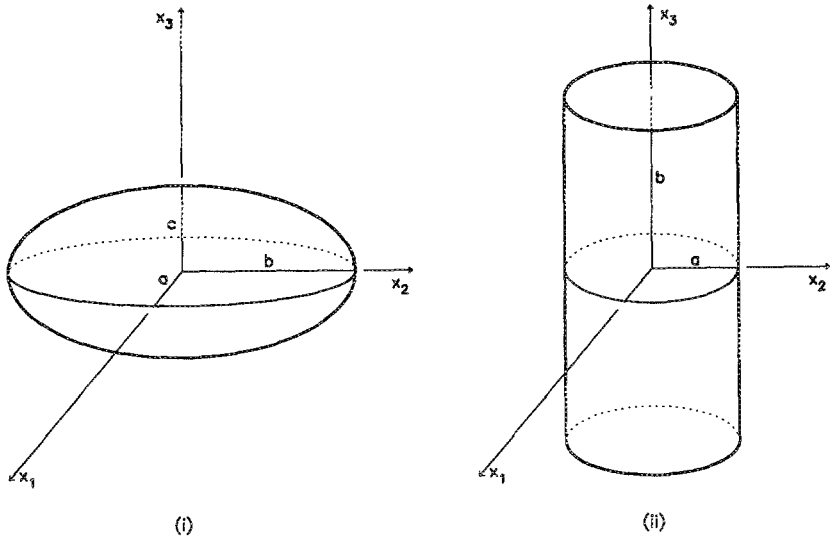

FIG. 2. Examples of three-dimensional inclusions: (i) Ellipsoid with axes of lengths 2a, 2b, and 2c; (ii) circular cylinder of diameter 2a and length 2b.

$$A(r) = 2a^2\left(\cos^{-1}\frac{r}{2a} - \frac{r}{2a}\sqrt{1-\frac{r^2}{4a^2}}\right)H(2a-r) \tag{42}$$

is the intersection area of two circles of radius a whose centers are separated by the distance r and $H(r)$ is the Heaviside step function. In Eq. (40), x and y are the distances between the centroids of two rectangular regions in the x_1 and x_2 directions, respectively. In Eq. (41), x is the magnitude of $\mathbf{x}$ and θ is the polar angle that $\mathbf{x}$ makes with the x_3 axis.

C. Overlapping oriented inclusions

As noted earlier, for overlapping inclusions $\rho_n(\mathbf{r}^n) = \rho^n$ and Eq. (31) exactly yields

$$S_n^{(1)}(\mathbf{x}_{12},\ldots,\mathbf{x}_{1n}) = 1 + \sum_{k=1}^{\infty}\frac{(-1)^k\rho^k}{k!}\int\prod_{j=1}^{n} \times\left(1-\prod_{i=1}^{k}[1-m(\mathbf{x}_i-\mathbf{r}_j)]\right)d\mathbf{r}_j. \tag{43}$$

Now the result of the previous subsection gives

$$S_n^{(1)}(\mathbf{x}_{12},\ldots,\mathbf{x}_{1n}) = 1 + \sum_{k=1}^{\infty}\frac{(-1)^k\rho^k}{k!}V_n(\mathbf{x}_{12},\ldots,\mathbf{x}_{1n}) = \exp[-\rho V_n(\mathbf{x}_{12},\ldots,\mathbf{x}_{1n})], \tag{44}$$

where, as before, V_n is the union volume of n inclusion regions. Note that Eq. (44) is exact and has an especially simple function form. Nonetheless, overlapping distributions of inclusions are quite complicated topologically, e.g., there is a critical inclusion volume fraction at which the included phase becomes connected (i.e., the percolation transition). This critical volume fraction occurs at a value well below the maximum (i.e., $\phi_2 = 1$). This is to be contrasted with distributions of impenetrable inclusions in which the critical point coincides with the maximum, random close-packing volume fraction.

D. Nonoverlapping oriented inclusions

For nonoverlapping inclusions, the ρ_n are generally very complicated. Here we shall state some general results for such models. First we note, as in the case of d-dimensional impenetrable spheres,[16] the infinite series (31) for nonoverlapping oriented inclusions truncates after the nth term in the sum because of the impenetrability condition, i.e., any term in the sum of series (31) for which $k > n$ is identically zero.

It is instructive to write the $S_n^{(1)}$ for impenetrable inclusions explicitly for $n = 1$ and 2. Equation (31) yields the matrix one-point probability function to be given exactly by

$$S_1^{(1)}(\mathbf{x}_1) = 1 - \int\rho_1(\mathbf{r}_1)m(\mathbf{x}_1-\mathbf{r}_1)d\mathbf{r}_1. \tag{45}$$

For homogeneous distributions, this becomes

$$S_1^{(1)} = \phi_1 = 1 - \rho V_1, \tag{46}$$

where it is to be recalled that V_1 is the volume of an inclusion. In contrast, Eq. (44) yields

$$S_1^{(1)} = \phi_1 = \exp(-\rho V_1) \tag{47}$$

for overlapping inclusions. To order ρ, the previous two relations are identical. For nondilute distributions, the higher-order terms in Eq. (44) account for corrections due to overlap, i.e., overlapping inclusions, at the same number density ρ, will always occupy less space than nonoverlapping inclusions at nondilute conditions. In other words, the matrix volume fraction ϕ_1 for overlapping inclusions is always greater than or equal to ϕ_1 for nonoverlapping inclusions at fixed ρ.

The two-point probability function for such anisotropic but homogeneous models is exactly given by

$$S_2^{(1)}(\mathbf{x}_{12}) = 1 - \rho V_2(\mathbf{x}_{12}) + \rho^2\int\rho_2(\mathbf{r}_{12})m(\mathbf{x}_1-\mathbf{r}_1) \times m(\mathbf{x}_2-\mathbf{r}_2)d\mathbf{r}_1\,d\mathbf{r}_2. \tag{48}$$

The two-body integrals appearing in (31) but not in (48) are

identically zero for the same reasons why the infinite series is truncated for impenetrable particles. In order to compute (48) one must know the two-particle probability density function: a quantity that has been studied extensively in liquid-state theory.[25] Thus, the theoretical machinery exists to compute $S_2^{(1)}$ for nontrivial models involving distributions of impenetrable, oriented inclusions.

IV. APPLICATIONS FOR DISTRIBUTIONS OF ORIENTED, OVERLAPPING CYLINDERS

A. Evaluation of the two-point microstructural parameters

We now consider computing the two-point microstructural parameter A_2 or, equivalently, $\mathsf{a}_2^{(i)}$ (henceforth denoted by a_2) for three-dimensional distributions of identical, oriented overlapping circular cylinders of finite aspect ratio b/a. Such a calculation enables us to compute expansion (3) through order β_{ij}^2, expansion (11) through order δ_{ij}^2, and the second-order bounds as expressed by relation (18). It is important to emphasize that the two-point tensors are the lowest-order parameters that reflect anisotropic or directional information about the composite. Recall that for macroscopically isotropic media,

$$\mathsf{A}_2 = \mathsf{O}, \quad \mathsf{a}_2 = [(-\phi_1\phi_2)/d\,]\mathsf{U}, \quad \mathsf{A}_2^* = (1/d)\mathsf{U}. \tag{49}$$

For any three-dimensional distribution of inclusions aligned in the x_3 direction which possesses transverse isotropy and azimuthal symmetry (e.g., circular cylinders, spheroids, etc.), we find from Eqs. (5), (10), and (13) that

$$\mathsf{a}_2 = -\phi_1\phi_2\mathsf{A}_2^* = -\phi_1\phi_2\begin{bmatrix} Q & 0 & 0 \\ 0 & Q & 0 \\ 0 & 0 & 1-2Q \end{bmatrix}, \tag{50}$$

where

$$Q = \frac{1}{3} - \lim_{\epsilon\to 0}\frac{1}{4\phi_1\phi_2}\int_\epsilon^\infty \frac{dx}{x}\int_0^\pi d\theta \sin\theta(1-3\cos^2\theta) \times [S_2^{(1)}(\mathbf{x}) - \phi_1^2]\,. \tag{51}$$

Here we have used spherical polar coordinates: x being the magnitude of $\mathbf{x}$ and θ being the polar angle measured with respect to the x_3 axis. The azimuthal angle is integrated out by virtue of the azimuthal symmetry possessed by $S_2^{(1)}(\mathbf{x})$ for such models. The diagonal elements $(a_2)_{11}$ and $(a_2)_{22}$ are equal because of isotropy in the x_1x_2 plane. Moreover, observe that the depolarization tensor appearing in (50) satisfies the general requirement that its trace be equal to unity; its diagonal components must also satisfy inequality (9b). Note that the integral of (51) gives the deviation from the isotropic result [cf. Eq. (49)].

For the specific case of *overlapping cylinders*, we have from (44), (47), and (51) that

$$Q = \frac{1}{3} - \lim_{\epsilon\to 0}\frac{\phi_1}{2\phi_2}\int_\epsilon^{x_{\max}}\frac{dx}{x}\int_0^1 du(1-3u^2) \times \exp[\rho V_2^{\text{int}}(x,u)\,], \tag{52}$$

$$V_2^{\text{int}}(x,u) = (2b-u)A(xv)H(2a-xv)H(2b-xu), \tag{53}$$

$$u = \cos\theta, \quad v = \sin\theta, \tag{54}$$

and

$$x_{\max} = 2\sqrt{b^2+a^2} \tag{55}$$

is the distance beyond which the function $S_2^{(1)}$ goes to its asymptotic value of ϕ_1^2. Here $V_2^{\text{int}}(\mathbf{x})$ is the intersection volume of two cylinders whose centroids are separated by $\mathbf{x}$ [as obtained from (41)] for the specified range of angles indicated in Eq. (52).

Before discussing the specific evaluation of the two-point microstructural parameter Q given by Eq. (52), it is first useful to make some general comments about it. First, it is clear that the microstructural parameter Q will generally depend upon the inclusion volume fraction ϕ_2 and the aspect ratio b/a, i.e., $Q = Q(\phi_2, b/a)$. Second, for certain aspect ratios, Q must take on known values. For example, from the discussion of Sec. II B, we know that for infinitely long cylinders ($b/a \to \infty$), the depolarization vanishes in the x_3 direction[26] and hence $1-2Q=0$ or $Q=1/2$. In the x_1x_2 plane, the problem effectively becomes *two-dimensional*, i.e., an isotropic distribution of overlapping disks, as can be seen by comparison to Eq. (49). In other words, the second-order bounds (18) in the x_1 and x_2 directions become the two-dimensional Hashin bounds.[21] On the other hand, we also know that for nonoverlapping, disk-shaped, plates of infinitesimal thickness,[26] $(A_2^*)_{11} = (A_2^*)_{22} = 0$ and $(A_2^*)_{33} = 1$. Therefore, for our overlapping-cylinder model in the limit $b/a \to 0$, $Q \to 0$ in the dilute limit. Strictly speaking, we must specify the dilute limit since it is only under such conditions that inclusion overlap can be neglected, i.e., to order ρ, $S_2^{(i)}$ is the same for both overlapping and nonoverlapping inclusions [cf. Eq. (39)]. Finally, we note that when the aspect ratio b/a is approximately unity, the microgeometry will be approximately statistically isotropic and $Q \cong 1/3$.

The microstructural parameter Q given by the integral (52) is numerically computed for our model of overlapping cylinders using a Gauss–Legendre quadrature. Our results as summarized in Table I where we give Q as a function of the aspect ratio b/a for values of the inclusion volume frac-

TABLE I. The microstructural parameter Q as a function of the aspect ratio b/a computed from Eq. (52) for aligned, overlapping cylinders and for aligned, nonoverlapping spheroids as obtained by Willis.[a]

	Microstructural parameter Q			
	Overlapping cylinders			Nonoverlapping spheroids
b/a	$\phi_2 = 0.1$	$\phi_2 = 0.5$	$\phi_2 = 0.9$	For all ϕ_2
0.0	0.000	0.000	0.000	0.000
0.01	0.0171	0.0179	0.0199	0.009
0.05	0.0617	0.0640	0.0693	0.037
0.10	0.102	0.105	0.111	0.070
0.20	0.160	0.163	0.169	0.125
0.50	0.263	0.264	0.266	0.236
1.00	0.344	0.343	0.340	0.333
2.00	0.409	0.407	0.402	0.413
5.00	0.460	0.458	0.454	0.472
10.00	0.480	0.478	0.475	0.490
20.0	0.490	0.489	0.487	0.497
100.00	0.498	0.498	0.498	0.500
∞	0.500	0.500	0.500	0.500

[a] See Ref. 10.

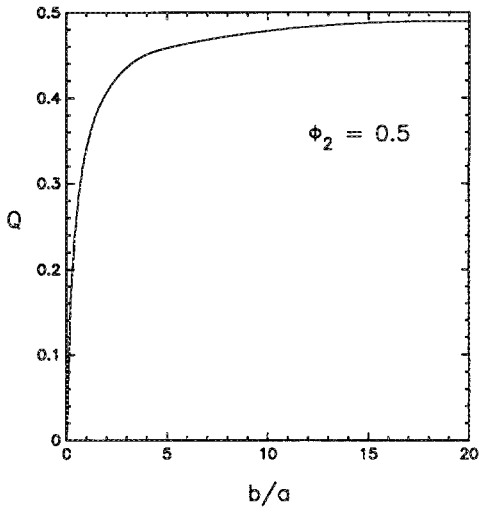

FIG. 3. Two-point microstructural parameter Q as a function of the aspect ratio b/a at $\phi_2 = 0.5$ for overlapping cylinders. Computed from Eq. (52). ϕ_2 is the cylinder volume fraction.

tion $\phi_2 = 0.1$, 0.5, and 0.9. Our numerical results for Q are seen to approach the aforementioned limiting values accurately. Observe that for fixed b/a, Q is a weak function of the volume fraction. Figure 3 depicts Q vs b/a for $\phi_2 = 0.5$.

In Table I we also include Q for the special geometry of nonoverlapping, spheroidal inclusions (aligned parallel to the x_3 axis with length $2b$ and maximum diameter of $2a$). These results, independent of ϕ_2, are obtained by comparing the general result (50) to the results of Willis[10] who specifically studied second-order bounds for this model. Note that for $b/a < 1$, Q for overlapping cylinders is greater than the corresponding quantity for nonoverlapping spheroids. For $b/a > 1$, the converse is true. This has important physical implications for the effective conductivity tensor as will be described below.

B. Perturbation expansion

Substitution of Eq. (50) into (11) gives the conductivity tensor exactly through order $\delta_{21}^2 = (\alpha - 1)^2$ to be

$$\frac{\boldsymbol{\sigma}_e}{\sigma_1} = \mathsf{U} + \phi_2 \mathsf{U}(\alpha - 1) - \phi_1\phi_2 \times \begin{bmatrix} Q & 0 & 0 \\ 0 & Q & 0 \\ 0 & 0 & 1-2Q \end{bmatrix} (\alpha - 1)^2, \tag{56}$$

where $\alpha = \sigma_2/\sigma_1$ is the ratio of the conductivity of the inclusions to that of the matrix. If $Q = 1/2$ and $\alpha > 1$, corresponding to conducting, infinitely long needles which are parallel to the x_3 direction, then from (56) it is clear that

$$(\sigma_e)_{11} = (\sigma_e)_{22} \leqslant (\sigma_e)_{33}. \tag{57}$$

On the other hand, if $Q = 0$ and $\alpha > 1$, corresponding to conducting, flat, disk-shaped plates oriented along the x_3 direction, then from (56) one has that

$$(\sigma_e)_{11} = (\sigma_e)_{22} \geqslant (\sigma_e)_{33}. \tag{58}$$

Similar results can be obtained for cases in which $\alpha < 1$.

For $b/a < 1$, the results of Table I and Eq. (56) lead one to conclude that $(\sigma_e)_{11}$ $[= (\sigma_e)_{22}]$ for nonoverlapping spheroids is larger than the corresponding quantity for overlapping cylinders at the same volume fraction. This is true despite the fact that in the latter case the inclusions can cluster to form a more connected included phase than in the former instance. However, for small aspect ratios, the *effective area fraction* of the included phase in the x_1x_2 plane in the case of nonoverlapping spheroids is larger than for the overlapping situation. For $b/a < 1$, this latter effect dominates over the former effect and hence explains the behavior of $(\sigma_e)_{11}$ $[= (\sigma_e)_{22}]$ for these microgeometries. On the other hand, for $b/a > 1$, the effective area fractions for the two models tend to approach ϕ_2 as b/a is made to increase. Hence, the connectedness of the cylinders in the x_1x_2 plane becomes a dominating effect and one arrives at the more obvious result, namely, that $(\sigma_e)_{11}$ $[= (\sigma_e)_{22}]$ for overlapping cylinders is greater than the corresponding conductivity for nonoverlapping spheroids.

It must be emphasized that the higher-order parameters $A_3^{(i)}$, $A_4^{(i)}$, etc., will be more sensitive to microstructural differences (as described above) than the two-point parameters. The higher-order parameters of course become increasingly important the more α differs from unity.

C. Second order bounds

Substitution of Eq. (50) into Eq. (18) leads to the second-order bounds

$$\frac{(\sigma_e^{(2)})_{11}}{\sigma_j} = \frac{(\sigma_e^{(2)})_{22}}{\sigma_j} = \frac{1 + (\phi_i + \phi_j Q)\delta_{ij}}{1 + \phi_j Q \delta_{ij}}, \tag{59}$$

$$\frac{(\sigma_e^{(2)})_{33}}{\sigma_j} = \frac{1 + [\phi_i + \phi_j(1-2Q)]\delta_{ij}}{1 + \phi_j(1-2Q)\delta_{ij}}. \tag{60}$$

For $\alpha = \sigma_2/\sigma_1 > 1$, (59) and (60) give lower bounds when $i = 2$ and $j = 1$ and upper bounds when $i = 1$ and $j = 2$.

As noted in Sec. II B 5, for cases in which one phase is much more conducting than the other (i.e., $\alpha \gg 1$ or $\alpha \ll 1$), the bounds will diverge from one another. Again, we emphasize that the bounds can still provide good estimates of the effective conductivity in such instances, even when $\alpha = \infty$ or $\alpha = 0$. For example, in the limit of perfectly conducting cylinders ($\alpha = \infty$), the upper bounds diverge to infinity and the lower bounds,

$$\frac{(\sigma_e^{(2L)})_{11}}{\sigma_1} = \frac{(\sigma_e^{(2L)})_{22}}{\sigma_1} = \frac{\phi_2 + \phi_1 Q}{\phi_1 Q}, \tag{61}$$

$$\frac{(\sigma_e^{(2L)})_{33}}{\sigma_1} = \frac{1 - 2\phi_1 Q}{\phi_1(1-2Q)}, \tag{62}$$

remain finite for $0 < \phi_2 < 1$, provided that $0 < Q < 1/2$. If $Q = 1/2$, then (as noted in Sec. II B 2) the second-order bounds in the x_3 direction, *for any α, coincide* (i.e., they are *exact*) and equal the first-order upper bound (17), which in the case $\alpha = \infty$ becomes infinite itself. Recall that $Q = 1/2$ corresponds to parallel slabs or infinitely long, cylinders in the x_3 direction. If $Q = 0$, corresponding to disk-shaped plates of infinitesimal thickness ($b/a = 0$), then the second-order bounds in the x_1- and x_2-directions, *for any α, coincide*

and again equal (17), which in the case $\alpha = \infty$ become infinite. From earlier discussions, therefore, we conclude that (61) and (62) will generally yield useful estimates of the diagonal components of the conductivity tensor $(\sigma_e)_{kk}$ provided that the conducting phase (phase 2) does not possess large *connected* substructures in the x_k direction. (As noted above, this provision need not always hold for the lower bound to be accurate.) A necessary but not sufficient condition for the conducting phase, in general, not to have large connected substructures is that it be below its percolation transition. We know, for example, that infinitely long, aligned cylinders percolate in the transverse plane at $\phi_2 \cong 0.68$.[27] This, therefore, is a lower bound on the percolation threshold in the *transverse plane* of aligned cylinders with a *finite* aspect ratio.

In the opposite limit of perfectly, insulating cylinders ($\alpha = 0$), the bounds again diverge. Let us scale the diagonal components of the conductivity tensor by σ_1 in this case. In the limit $\alpha \to 0$, then the scaled lower bounds go to zero and the scaled upper bounds

$$\frac{(\sigma_e^{(2U)})_{11}}{\sigma_1} = \frac{(\sigma_e^{(2U)})_{22}}{\sigma_1} = \frac{\phi_1(1-Q)}{1-\phi_1 Q}, \tag{63}$$

$$\frac{(\sigma_e^{(2U)})_{33}}{\sigma_1} = \frac{2\phi_1 Q}{\phi_2 + 2\phi_1 Q}, \tag{64}$$

remain finite. As before, the upper bounds generally will provide a good estimate of the effective conductivity given that the conducting phase (phase 1) is connected. Of course, if the conducting phase is disconnected, then the scaled lower bounds (equal to zero) are exact.

Figures 4 and 5 show bounds on the diagonal components of the scaled effective conductivity tensor $(\sigma_e/\sigma_1$ $[\sigma_e \equiv (\sigma_e)_{kk}]$ for a distribution of conducting cylinders ($\alpha = 10$) with $b/a = 10$ (slender, conducting rods) and

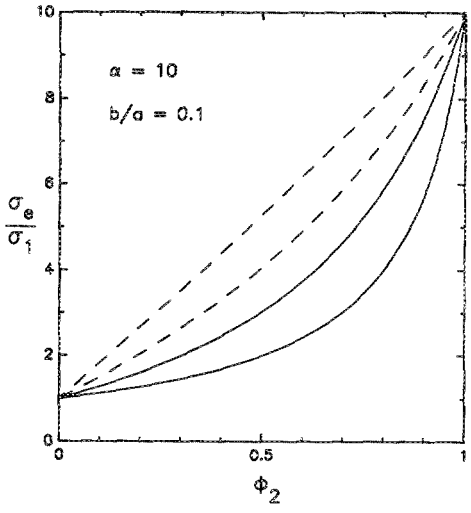

FIG. 5. As in Fig. 4 for a composite containing conducting ($\alpha = 10$), flat ($b/a = 0.1$) disks.

$b/a = 0.1$ (flat, conducting disks), respectively. For the case $\alpha = 10$ and $b/a = 10$, we see that inequality (57) is rigorously satisfied, i.e., the conductivity in the x_3 direction is always greater than the conductivity in the transverse plane. Note that for reasons mentioned earlier, the bounds on $(\sigma_e)_{33}$ are very sharp. Similarly, for $\alpha = 10$ and $b/a = 0.1$, inequality (58) is rigorously satisfied. Figures 6 and 7 depict bounds on σ_e/σ_2 for a distribution of insulating cylinders ($\alpha = 0.1$) with $b/a = 10$ (slender, insulating rods) and $b/a = 0.1$ (flat, insulating disks), respectively. Figure 8 shows *lower* bounds on the scaled conductivity components σ_e/σ_1 for a composite containing *perfectly conducting* ($\alpha = \infty$), very slender ($b/a = 20$) cylindrical in-

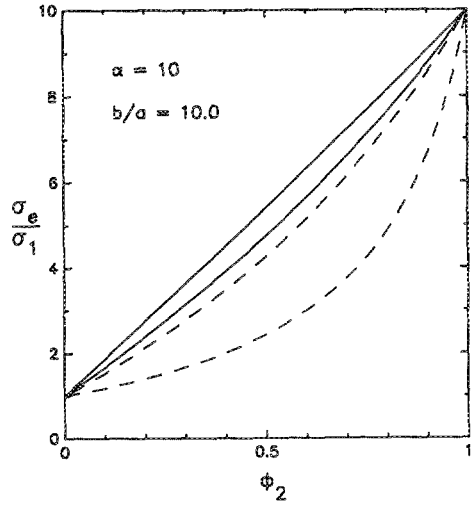

FIG. 4. Second-order bounds on the scaled conductivity components σ_e/σ_1 $[\sigma_e \equiv (\sigma_e)_{kk}]$ vs ϕ_2 for a composite containing conducting ($\alpha = 10$), slender ($b/a = 10$) cylindrical inclusions. The dashed lines (---) are bounds (59) for $(\sigma_e)_{11} = (\sigma_e)_{22}$ and solid lines (—) are bounds (60) for $(\sigma_e)_{33}$. Here ϕ_2 is the cylinder volume fraction, b/a is the aspect ratio, and $\alpha = \sigma_2/\sigma_1$ is the conductivity ratio.

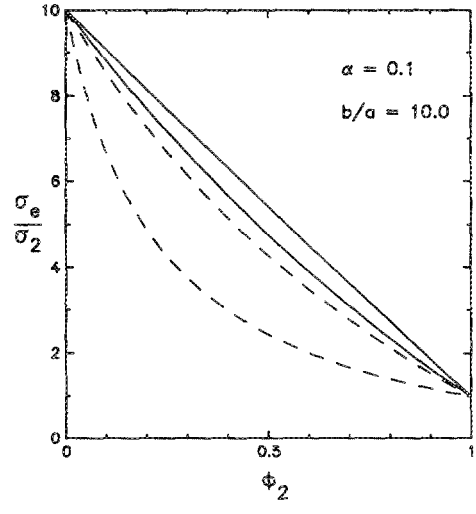

FIG. 6. Second-order bounds on the scaled conductivity components σ_e/σ_2 $[\sigma_e \equiv (\sigma_e)_{kk}]$ vs ϕ_2 for a composite containing nonconducting ($\alpha = 0.1$), slender ($b/a = 10$) cylindrical cavities. The dashed lines (---) are bounds (59) for $(\sigma_e)_{11} = (\sigma_e)_{22}$ and solid lines (—) are bounds (60) for $(\sigma_e)_{33}$.

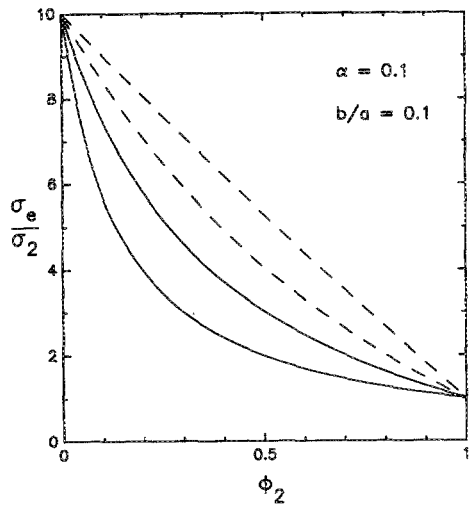

FIG. 7. As in Fig. 6 for a composite containing nonconducting ($\alpha = 0.1$), flat ($b/a = 0.1$) disk-shaped cavities.

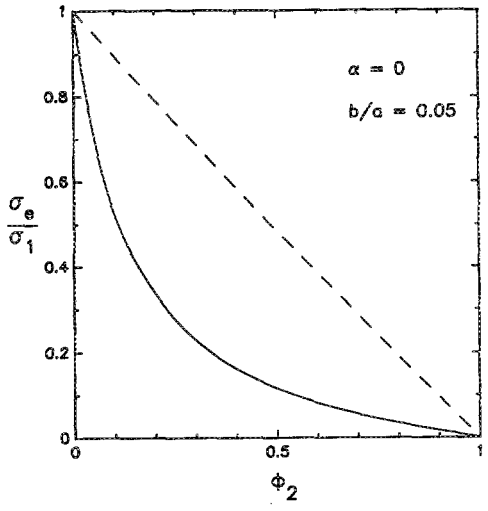

FIG. 9. Second-order upper bounds on the scaled conductivity components σ_e/σ_1 [$\sigma_e \equiv (\sigma_e)_{kk}$] vs ϕ_2 for a composite containing perfectly insulating ($\alpha = 0$), penny-shaped ($b/a = 0.05$) cracks. The dashed line (---) is the upper bound (63) for $(\sigma_e)_{11} = (\sigma_e)_{22}$ and the solid line (—) is the upper bound (64) for $(\sigma_e)_{33}$.

clusions. Figure 9 depicts *upper* bounds on the scaled conductivity components σ_e/σ_1 for a composite containing *perfectly insulating* ($\alpha = 0$), penny-shaped ($b/a = 0.05$) *cracks*.

V. CONCLUSIONS

We have given a general series representation of the n-point probability functions for statistically anisotropic media composed of identical, aligned inclusions of arbitrary shape distributed throughout a matrix. This enables one in principle to compute perturbation expansions and rigorous nth-order bounds for the effective conductivity tensor σ_e of such media. The formalism was applied by computing a second-order perturbation expansion and bounds for the microgeometry of aligned, overlapping cylinders of finite aspect ratio. We found that the two-point parameter involved Q [cf. Eq. (50)], which contains the simplest level of anisotropic information, was sensitive to the details of the microstructure. The bounds were shown to yield useful estimates of the effective conductivity tensor for a wide range of volume fractions, aspect ratios, and conductivity ratios, even when the bounds diverge.

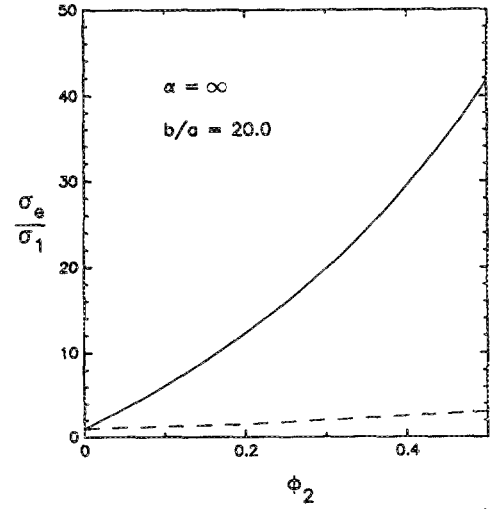

FIG. 8. Second-order *lower* bounds on the scaled conductivity components σ_e/σ_1 [$\sigma_e \equiv (\sigma_e)_{kk}$] vs ϕ_2 for a composite containing perfectly conducting ($\alpha = \infty$), very slender ($b/a = 20$), cylindrical inclusions. The dashed line (---) is the lower bound (61) for $(\sigma_e)_{11} = (\sigma_e)_{22}$ and the solid line (—) is the lower bound (62) for $(\sigma_e)_{33}$.

ACKNOWLEDGMENTS

The authors thank G. W. Milton for valuable comments. This research was supportd by the Office of Basic Energy Sciences, U.S. Department of Energy under Grant No. DE-FG05-86ER13842.

[1]J. C. Maxwell, *Treatise on Electricity and Magnetism* (Clarendon, Oxford, 1873).
[2]A. Einstein, Ann. Phys. **19**, 289 (1906).
[3]Lord Rayleigh, Philos. Mag. **34**, 481 (1892).
[4]G. W. Milton, Commun. Math. Phys. **III**, 281 (1987); **III**, 329 (1987).
[5]S. Torquato, Rev. Chem. Eng. **4**, 151 (1987).
[6]See also references given in Refs. 4 and 5.
[7]W. F. Brown, J. Chem. Phys. **23**, 1514 (1955).
[8]A. Rocha and A.Acrivos, *Q. J. Mech. Appl. Mech.* **26**, 441 (1973). We should note that approximations for the conductivity tensor of a nondilute suspension of very slender, aligned rods were obtained by A. Acrivos and E. S. G. Shaqfeh, Phys. Fluids **31**, 1841 (1988) and E. S. G. Shaqfeh, Phys. Fluids **31**, 2405 (1988).
[9]M. Hori, J. Math. Phys. **14**, 514 (1973); **14**, 1942 (1973); **16**, 365 (1975).
[10]J. R. Willis, J. Mech. Phys. **25**, 185 (1977).
[11]R. V. Kohn and G. W. Milton, in *Homogenization and Effective Moduli of Materials and Media*, edited by J. Ericksen, D.Kinderlehrer, R. Kohn, and J. L. Lions (Springer, Berlin, 1986).
[12]A. K. Sen and S. Torquato, Phys. Rev. B **39**, 4504 (1989).
[13]Hori (Ref. 9) derived a different series expansion, having coefficients which depend upon *derivatives* of n-point correlation functions. He also derived bounds which depend upon the same coefficients. In practice, one measures the correlation functions themselves, not their derivatives. Un-

like the n-point integrals $A_n^{(i)}$, the corresponding integrals are generally conditionally convergent.
[14]G. W. Milton, in *Homogenization and Effective Moduli of Materials and Media*, edited by J. Ericksen, D. Kinderlehrer, R. Kohn, and J. L. Lions (Springer, Berlin, 1986).
[15]P. B. Corson, J. Appl. Phys. **45**, 3159 (1974); **45**, 3165 (1974). Using a painstaking procedure, Corson measured two- and three-point probability functions of two-phase metal mixtures.
[16]S. Torquato and G. Stell, J. Chem. Phys. **77**, 2071 (1982).
[17]S. Torquato and G. Stell, J. Chem. Phys. **79**, 1505 (1983); **82**, 980 (1985); S. Torquato and F. Lado, J. Phys. A **18**, 141 (1985); S. Torquato, J. Stat. Phys. **45**, 843 (1986); Phys. Rev. B **35**, 5385 (1987).
[18]J. G. Berryman, J. Appl. Phys. **57**, 2374 (1985); J. G. Berryman and S. C. Blair, J. Appl. Phys. **60**, 1930 (1986). These authors efficiently measure lower-order correlation functions using image processing techniques.
[19]S. Toquato and G. Stell, Lett. Appl. Eng. Sci. **23**, 375 (1985); S. Torquato and J. D. Beasley, Int. J. Eng. Sci. **24**, 435 (1986); C. G. Joslin and G. Stell, J. Appl. Phys. **60**, 1607 (1986); S. Torquato and F. Lado, Phys. Rev. B **33**, 6248 (1986); S. Torquato and J. D. Beasley, Phys. Fluids **30**, 633 (1987); A. K. Sen, F. Lado, and S. Torquato, J. Appl. Phys. **62**, 4135 (1987); S. Torquato and F. Lado, Proc. R. Soc. London Ser. A **417**, 59 (1988).
[20]O. Wiener, Abh. Math. Phys. Kl. Kgl. Sächs. Ges. **32**, 509 (1912).
[21]Z. Hashin and S. Shtrikman, J. Appl. Phys. **33**, 3125 (1962).
[22]M. Beran, Nuovo Cimento **38**, 771 (1965).
[23]N. Silnutzer, Ph.D. thesis, University of Pennsylvania, Philadelphia, PA, 1972.
[24]G. W. Milton, J. Appl. Phys. **52**, 5294 (1981).
[25]J. P. Hansen and I. R. McDonald, *Theory of Simple Liquids* (Academic, London, 1986).
[26]These limiting values can be obtained from the well-known depolarization factors for an ellipsoid. In Ref. 12, relations (4.7) and (4.8) are the general depolarization factors for an ellipse and ellipsoid, respectively. Note that the term $t + a_i$ appearing in both of these equations should read $t + a_i^2$.
[27]S. W. Haan and R. Zwanzig, J. Phys. A **10**, 1547 (1977), and references therein.